PAPER

Check for updates

A novel approach for estimating the strength of argentophilic and aurophilic interactions using QTAIM parameters†

Sergi Burguera, [ID] Antonio Bauzá [ID] and Antonio Frontera [ID] *

Metallophilic interactions, specifically argentophilic (Ag···Ag) and aurophilic (Au···Au) interactions, play a crucial role in stabilizing various molecular and solid-state structures. In this manuscript, we present a convenient method to estimate the strength of argentophilic and aurophilic interactions based on quantum theory of atoms in molecules (QTAIM) parameters evaluated at the bond critical points connecting the metal centres. We employ density functional theory (DFT) calculations and the QTAIM parameters to develop this energy predictor. To validate the reliability and applicability of our method, we test it using a selection of X-ray crystal structures extracted from the cambridge structural database (CSD), where argentophilic and aurophilic interactions are known to be significant in their solid-state arrangements. This method offers a distinct advantage in systems where multiple interactions, beyond metallophilic interactions, contribute to the overall stability of the structure. By employing our approach, researchers can distinctly quantify the strength of argentophilic and aurophilic interactions, facilitating a deeper understanding of their impact on molecular and solid-state properties. This method fills a critical gap in the existing literature, offering a valuable tool to researchers seeking to unravel the intricate interactions in metal-containing compounds.

Introduction

In the realm of supramolecular chemistry, the understanding and rational utilization of non-covalent interactions is fundamental to the development of novel materials and molecular systems.[1] Among these non-covalent interactions, argentophilic[2] and aurophilic[3] interactions have emerged as areas of significant interest due to their unique properties and potential applications.[2,3] Several reviews have provided a comprehensive overview of argentophilic and aurophilic interactions, delving into their nature, characteristics, and the pivotal role they play in several fields.[2–10]

Argentophilic interactions are predominantly observed in silver(I) complexes, where the d^{10} configuration of silver plays a crucial role.[4] The relatively large atomic radius of silver facilitates these interactions, which are often compared to hydrogen bonding in terms of their strength. Similarly, aurophilic interactions involve gold atoms and are particularly notable in gold(I) and gold(III) complexes. These interactions are attributed

to the relativistic effects on the gold atoms, where the contraction of the 6s orbital and expansion of the 5d orbital lead to distinctive electron configurations conducive to bonding.[11–15] Aurophilic interactions are not only intriguing from a theoretical standpoint but also have substantial implications in the design of luminescent materials[16–20] and catalysts.[21] Both argentophilic and aurophilic interactions contribute to the stability and function of metallo-supramolecular complexes.[22] In recent years, these interactions have been harnessed in the creation of porous materials,[23] sensors,[24] spintronics,[25] and in medicinal chemistry, particularly in the development of anticancer and antimicrobial agents.[26]

In the intricate field of crystal engineering, argentophilic and aurophilic interactions have emerged as pivotal forces, offering novel avenues for the design and synthesis of complex crystal structures.[27] These interactions are particularly significant due to their ability to influence and stabilize the geometrical arrangement of atoms within a crystal lattice, a fundamental aspect in tailoring the properties of materials.[28] The directional nature of these metallophilic interactions enables the precise arrangement of molecular components, leading to highly ordered and more predictable crystal structures.[29,30] This control is crucial in the creation of porous networks, which have applications in gas storage, separation technologies, and catalysis.[21,23,24] Additionally, the luminescent

Department of Chemistry, Universitat de les Illes Balears, Crta de Valldemossa km 7.5, 07122 Palma de Mallorca (Baleares), Spain. E-mail: toni.frontera@uib.es

† Electronic supplementary information (ESI) available: X-ray coordinates and correlation plots without relativistic effects and multivariant details. See DOI: https://doi.org/10.1039/d4cp00410h

16550 | *Phys. Chem. Chem. Phys.*, 2024, **26**, 16550–16560

This journal is © the Owner Societies 2024

properties induced by aurophilic interactions are being exploited in the development of new optoelectronic materials, pushing the boundaries of what is achievable in crystal engineering.[31]

Argentophilic and aurophilic interactions are distinguished by their unique physical nature, which arises from the specific electronic configurations of silver and gold atoms.[11–15] These metallophilic interactions, while being a subset of van der Waals forces, are nuanced and multifaceted in nature. Apart from important relativistic effects, these interactions commonly exhibit electrostatic repulsion that is compensated by dispersion forces.[2,3] They are especially relevant due to the involvement of large, polarizable electron clouds in both silver and gold atoms. The larger atomic size and the extensive electron cloud of these heavy atoms enhance the strength of dispersion forces, contributing significantly to the overall stabilization.

This manuscript introduces a convenient methodology for estimating the strength of argentophilic and aurophilic interactions, utilizing the quantum theory of atoms in molecules (QTAIM) and electron density properties at bond critical points between metal centers. Leveraging DFT calculations in conjunction with QTAIM parameters, we have developed an energy predictor model. This model enables the estimation of interaction strengths for $Ag(I)\cdots Ag(I)$ and $Au(I)\cdots Au(I)$ bonds without necessitating separate calculations for the individual monomers. The practicality of our approach has been validated through analysis of a selection of X-ray crystal structures sourced from the cambridge structural database (CSD), focusing on structures where argentophilic and aurophilic interactions are integral to their solid-state arrangements. The method offers a significant advantage in evaluating the contribution of metallophilic interactions in systems with multiple contributing interactions and in molecular assemblies where the interactions are intramolecular. By applying our technique, researchers can efficiently estimate the strength of argentophilic and aurophilic interactions. This quantification is crucial for understanding and predicting the influence of these interactions on both molecular and solid-state properties, providing a valuable tool for advancements in the field of supramolecular chemistry and material science.

Theoretical methods

The monomers from the studied complexes were firstly optimized at the PBE0-x2c[32]-D4[33]/x2c-TZVPall[34] and PBE0-D4/def2-TZVP levels of theory using a fine grid. The def2-TZVP basis set uses ECPs for Ag and Au atoms.[34–36] Relativistic quantum chemistry is essential for properly understanding the chemistry of heavy and super-heavy elements and their compounds, as these effects largely determine their electronic structures, properties, and functions. Relativistic exact decoupling can be achieved using either the x2c (exact two-component) approach or the BSS (Barysz–Sadlej–Snijders) approach. The x2c approach is recommended because it is simpler, avoiding the additional free-particle Foldy–Wouthuysen transformation required by the

BSS approach.[32b] For comparison, we have also used the def2-TZVP basis set, which employs effective core potentials (ECPs). The use of ECPs for heavier atoms is popular for good reasons: it reduces the number of basis functions and, consequently, the computational workload; at the same time, it also accounts for scalar relativistic effects.[34–36] The D4 dispersion correction was selected for its ability to provide an accurate, efficient, and particularly robust description of metals.[33b]

Then, for PBE0-x2c-D4/x2c-TZVPall and PBE0-D4/def2-TZVP levels of theory, the homodimers were studied through a first "rough" scan of 0.1 Å of step size on the $Ag\cdots Ag$ or $Au\cdots Au$ distance along the main symmetry axis until a minimum was found. The linear ligands were set perpendicular to each other to minimize ancillary interactions. Once the minimum was found, a "refined" scan was performed to better approach the real minimum using 0.0125 Å of step size, moving one Å in each direction from the minimum. The scans were performed as single point calculations at the same level of theory as the monomer optimizations using the Turbomole 7.7 program.[37] The minimum geometry was then further analysed by means of Bader's Quantum Theory of Atoms in Molecules[38] at the same level of theory. In all cases, a bond critical point (BCP) was found interconnecting the Regium atoms ($Ag\cdots Ag/Au\cdots Au$) and its electron density and derivatives of the latter were subtracted and analysed, using the Multiwfn software.[39]

Results and discussion

X-ray examples

Fig. 1 shows some selected examples of X-ray structures retrieved from the CSD where argentophilic interactions are present and have a structural directing role. For instance, in **BIQWEF**[40] structure (Fig. 1a) the (μ_2-ethane-1,2-diamine)-dichloro-di-silver(I) molecules propagate forming 1D polymers via the formation of $Ag\cdots Ag$ interactions in combination with H-bonding interactions. 1D infinite assemblies are also observed in **HAMMIS**[41] and **LURDIM**[42] structures, both are diammine-silver(I) salts (counteranions are omitted for clarity) that form either symmetric (**HAMMIS**) or asymmetric $Ag\cdots Ag$ interactions (**LURDIM**).

Additional examples comprise discrete dimers formed in (pyrazine N-oxide)-(trifluoroacetato)-silver(I) (**POKHEE**)[43] and benzylamino-chloro-silver(I) (**YUXVUJ**)[44] structures (Fig. 1d and e). In **BURVER**[45] (Fig. 1f), two Ag(I) ions promote the formation of a macrocycle by connecting two μ-4,4′-(1,2-phenylenebis(methylene-sulfanediyl))bispyridine units via Ag–N coordination bonds. The Ag(I) metals are separated 3.236 Å, thus establishing an intramolecular interaction. This distance is similar to the intermolecular distances observed in the rest of X-ray structures supporting its structural-directing role.

The evaluation of the strength of the argentophilic interactions by the traditional supramolecular approach is complicated in all these examples. For instance, in neutral systems like **BIQWEF**, **POKHEE** and **YUXVUJ** additional interactions are established, therefore calculation of the dimerization energies

This journal is © the Owner Societies 2024

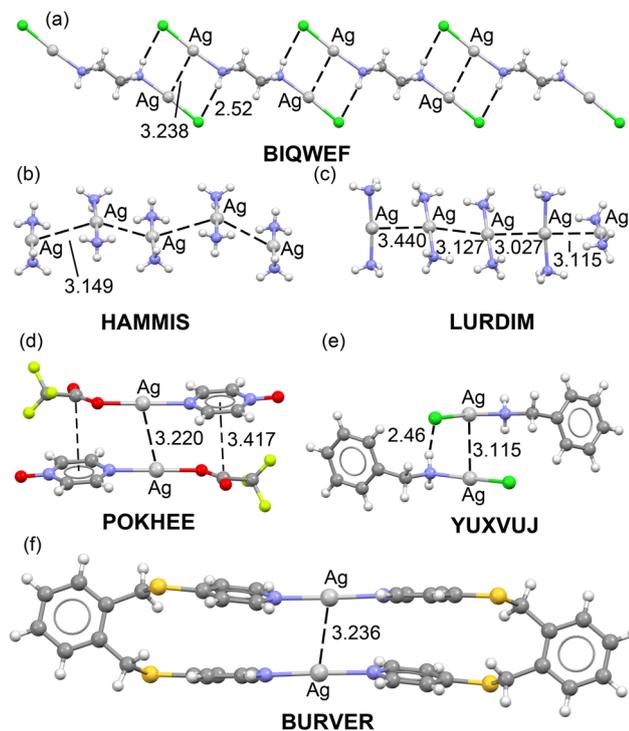*Phys. Chem. Chem. Phys.*, 2024, **26**, 16550–16560 | **16551**

Fig. 1   X-ray solid state structures of CSD codes **BIQWEF** (a), **HAMMIS** (b), **LURDIM** (c), **POKHEE** (d), **YUXVUJ** (e) and **BURVER** (f). In **HAMMIS**, **LURDIM** and **BURVER** the counterions are omitted. Distances in Å.
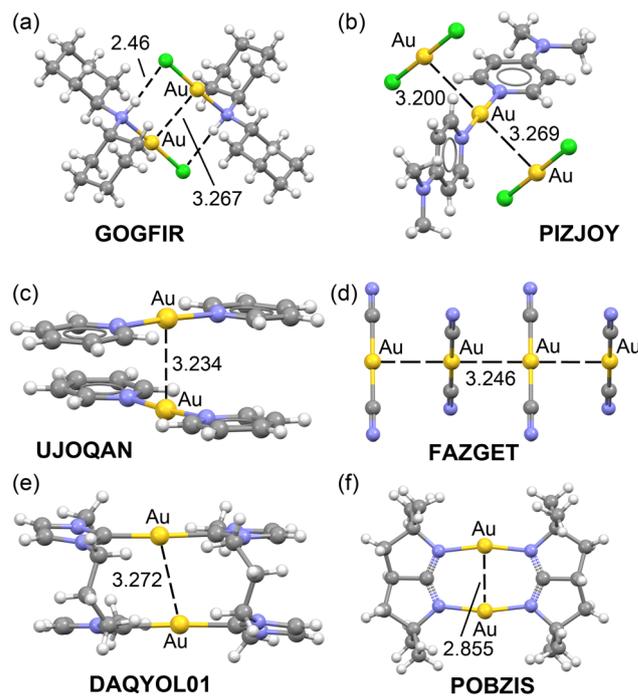

Fig. 2   X-ray solid state structures of CSD codes **GOGFIR** (a), **PIZJOY** (b), **UJOQAN** (c), **FAZGET** (d), **DAQYOL01** (e) and **POBZIS** (f). The counterions are omitted.

is not useful to extract the contribution of the argentophilic interaction.

In other structures like **HAMMIS** or **LURDIM**, the positive charge of the monomer Ag(NH$_3$)$_2^+$ anticipates a repulsive interaction due to the dominant coulombic cation···cation repulsion in the dimer. Again, difficult to extract the stabilizing contribution from the argentophilic interactions. Finally, in **BURVER** compound, it is even more complicated, since in addition to the electrostatic repulsion, the contact is intramolecular.

A similar situation is anticipated in Au(ɪ) X-ray structures exhibiting aurophilic interactions. A selection of structures is given in Fig. 2. The **GOGFIR**[46] structure (Fig. 2a) forms self-assembled dimers where the chloro-bis(dicyclohexylamine)-gold(ɪ) monomers establish both Au···Au and H-bonding interactions. The **PIZJOY**[47] structure (Fig. 2b) forms 1D infinite assemblies where cationic bis(4-(dimethylamino)pyridine)-gold(ɪ) and anionic dichloro-gold(ɪ) are arranged *via* the formation of Au···Au interactions. The **UJOQAN**[48] structure (Fig. 2c) forms cation···cation dimers in the solid state where the monomers are rotated 90°. In **FAZGET**,[49] the dicyano-gold(ɪ) monomers propagate in the solid state forming 1D assemblies (see Fig. 2d). Finally, two additional examples of intramolecular Au···Au interactions are provided in Fig. 2, bottom (**DAQYOL01**[50] and **POBZIS**[51]). In one of them (**DAQYOL01**) the Au···Au distance is comparable to those observed in the intermolecular assemblies while in the other one (**POBZIS**) it is considerably shorter due to the rigidity of the (μ-$_{2,2,5,5}$-tetramethyl-1,2,3,3a,4,5-hexahydro-pyrrolo[2,3-*b*]pyrrole) ligand.

The evaluation of the aurophilic interactions is complicated in these structures, either because of the ancillary interactions or the ionic nature of the monomers. That is, anion···anion in **FAZGET**, cation···cation in **UJOQAN** or anion···cation in **PIZJOY**. In these three cases the dimerization energies would be dominated by strong repulsive (**FAZGET** and **UJOQAN**) or strong attractive (**PIZJOY**) coulombic forces, thus complicating the evaluation of the real strength of the Au···Au interaction even in the absence of secondary interactions.

Theoretical study

To effectively evaluate the significance and intensity of metallophilic Ag···Ag and Au···Au interactions in complex supramolecular systems, particularly those with multiple noncovalent interactions or charged constituents, we propose employing Bader's Quantum Theory of Atoms in Molecules (QTAIM) analysis. This approach is especially advantageous for scenarios where distinguishing individual interaction contributions is otherwise challenging. QTAIM analysis focused on bond critical point properties allows for a more detailed and precise assessment of these intricate bonding scenarios.

For hydrogen, halogen, and chalcogen bonds, the use of electronic potential energy density (V) and Lagrangian kinetic energy density (G) has been previously suggested.[52–58] These parameters have been explored in molecular crystals, with G recommended for hydrogen bonds and V for halogen and chalcogen bonds.[59] However, to our knowledge, the application of these parameters has not been developed or tested for Ag···Ag or Au···Au interactions.
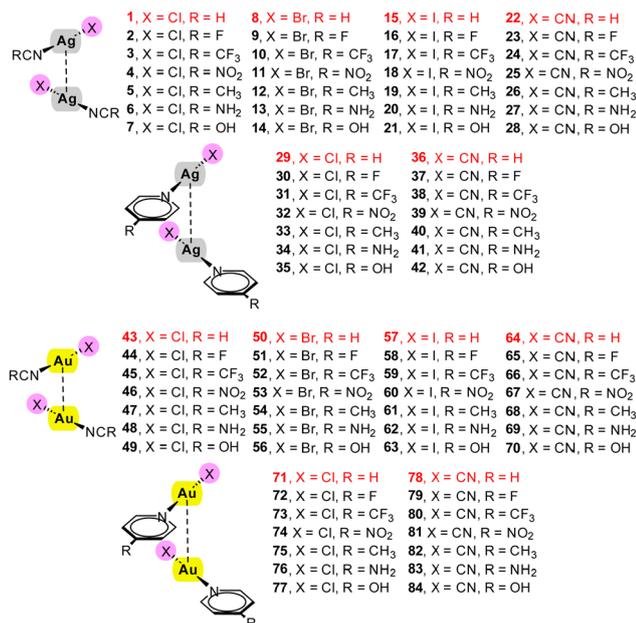
Scheme 1 Homodimers **1–84** studied in this work and their numbering. In red those complexes used to validate the equations and not used to construct the regression plots.

In this section, we aim to provide a straightforward method for estimating the strength of Ag···Ag and Au···Au interactions. Utilizing the set of complexes outlined in Scheme 1, we have calculated the dimerization energies, conducted QTAIM analysis, and extracted relevant QTAIM parameters at the BCPs connecting the noble metal atoms.

Silver complexes

The characteristics and topological parameters for complexes **1–42** are detailed in Table 1. For these complexes, a linear mode of complexation, specific ligands, and a relative orientation of the monomers at a 90° rotation in the dimer were chosen. This configuration was selected to minimize secondary interactions and to reflect ligand arrangements typically observed in solid-state structures. Importantly, the chosen monomers are neutral, thus ensuring that pure coulombic forces (either attractive or repulsive) are not predominant in these systems. Additionally, we utilized scans instead of fully optimized geometries to maintain the complexes in a 'frozen' state, preventing the formation of secondary interactions. This approach allows us to attribute the calculated dimerization energy (the energy of the homodimer minus twice the energy of the monomer) directly to the strength of the metallophilic contact. Fully optimization of the complexes leads to an antiparallel orientation with ligand···ligand interactions.

To illustrate our methodology, we showcase the energy profiles for two representative dimers of silver and gold (**4** and **83**) in Fig. 3. For these profiles, frozen scans (using the optimized geometries of the monomers) were employed to vary the Rg···Rg distance and thereby extract the energy profiles. This approach has been consistently applied across dimers **1–84** as reported in our study.

Table 1 Dimerization energy (kcal mol⁻¹), distances (d, Å), ρ (a.u.), $\nabla^2\rho$ (a.u.), potential energy density (V, a.u.) and Lagrangian kinetic energy (G, a.u.) for complexes **1–42** at the PBE0(x2c)-D4/x2c-TZVPall level of theory

Dimer	E^a	d	ρ	$\nabla^2\rho$	V	G
1	−6.06 (−6.16)	3.038	0.0202	0.0575	−0.0155	0.0149
2	−6.46 (−6.57)	3.013	0.0212	0.0607	−0.0167	0.0159
3	−6.56 (−6.67)	3.025	0.0208	0.0591	−0.0161	0.0155
4	−6.49 (−6.58)	3.013	0.0213	0.0607	−0.0167	0.0160
5	−5.86 (−6.00)	3.038	0.0201	0.0576	−0.0155	0.0149
6	−5.35 (−5.50)	3.038	0.0200	0.0577	−0.0154	0.0149
7	−6.03 (−6.16)	3.025	0.0206	0.0592	−0.0161	0.0154
8	−6.80 (−6.77)	3.013	0.0213	0.0605	−0.0168	0.0159
9	−7.24 (−7.22)	2.988	0.0223	0.0638	−0.0181	0.0170
10	−7.35 (−7.34)	3.000	0.0219	0.0622	−0.0174	0.0165
11	−7.29 (−7.26)	3.000	0.0219	0.0621	−0.0174	0.0165
12	−6.59 (−6.60)	3.013	0.0212	0.0606	−0.0167	0.0159
13	−6.07 (−6.08)	3.025	0.0206	0.0590	−0.0161	0.0154
14	−6.79 (−6.79)	3.013	0.0211	0.0605	−0.0167	0.0159
15	−8.08 (−7.80)	3.000	0.0219	0.0620	−0.0174	0.0165
16	−8.56 (−8.28)	2.975	0.0230	0.0655	−0.0188	0.0176
17	−8.71 (−8.45)	2.988	0.0218	0.0622	−0.0174	0.0165
18	−8.62 (−8.34)	2.988	0.0226	0.0636	−0.0181	0.0170
19	−7.88 (−7.65)	3.000	0.0218	0.0622	−0.0174	0.0165
20	−7.34 (−7.12)	3.013	0.0212	0.0605	−0.0167	0.0159
21	−8.02 (−7.79)	3.000	0.0218	0.0621	−0.0174	0.0164
22	−5.40 (−5.48)	3.075	0.0192	0.0530	−0.0141	0.0137
23	−5.60 (−5.64)	3.063	0.0197	0.0544	−0.0146	0.0141
24	−5.67 (−5.77)	3.050	0.0202	0.0560	−0.0152	0.0146
25	−5.54 (−5.62)	3.050	0.0203	0.0559	−0.0152	0.0146
26	−5.45 (−5.54)	3.075	0.0192	0.0531	−0.0140	0.0136
27	−5.08 (−5.18)	3.075	0.0191	0.0532	−0.0140	0.0136
28	−5.57 (−5.66)	3.063	0.0196	0.0546	−0.0145	0.0141
29	−10.22 (−10.31)	2.925	0.0254	0.0739	−0.0221	0.0203
30	−10.45 (−10.54)	2.925	0.0254	0.0739	−0.0221	0.0203
31	−10.53 (−10.65)	2.925	0.0255	0.0738	−0.0221	0.0203
32	−10.62 (−10.72)	2.925	0.0255	0.0738	−0.0221	0.0203
33	−9.77 (−9.89)	2.938	0.0248	0.0718	−0.0213	0.0196
34	−9.31 (−9.44)	2.925	0.0253	0.0739	−0.0220	0.0203
35	−10.02 (−10.13)	2.925	0.0254	0.0739	−0.0221	0.0203
36	−9.68 (−9.73)	2.963	0.0241	0.0681	−0.0199	0.0185
37	−9.60 (−9.67)	2.963	0.0241	0.0681	−0.0199	0.0185
38	−9.35 (−9.44)	2.975	0.0236	0.0662	−0.0192	0.0179
39	−9.54 (−9.61)	2.963	0.0242	0.0681	−0.0200	0.0185
40	−9.29 (−9.37)	2.963	0.0241	0.0681	−0.0199	0.0185
41	−9.21 (−9.30)	2.963	0.0240	0.0682	−0.0199	0.0185
42	−9.53 (−9.60)	2.963	0.0240	0.0682	−0.0199	0.0185

^{a} Values in parenthesis correspond to PBE0-D4/def2-TZVP level of theory. The repression plots for this level of theory are included in the ESI, Fig. S1.
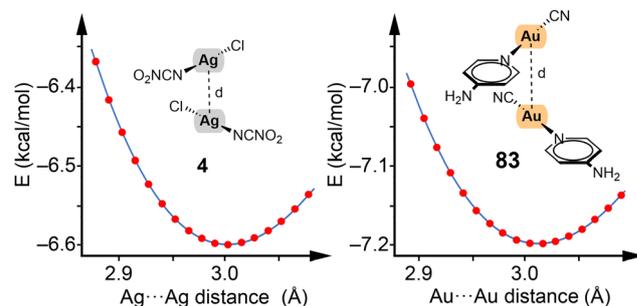

Fig. 3 Energy profiles constructed using frozen scans for complexes **4** and **83**. Energy in kcal mol⁻¹ and distances in Å.

The minimum energy geometries identified from these profiles were further analysed using QTAIM to obtain parameters

Table 2 Dimerization energies (kcal mol^{-1}) of complexes (**1**, **8**, **15**, **22**, **29** and **36**) using the scan plots (E) and eqn (1). The differences (ΔE, absolute values) are also indicated given

Dimer	E	E (eqn (1))	$|\Delta E|^a$
1	−6.06	−6.01	0.05
8	−6.80	−6.92	0.12
15	−8.08	−7.47	0.61
22	−5.40	−5.20	0.21
29	−10.22	−10.44	0.22
36	−9.68	−9.32	0.36

^{a} SD = 0.31 kcal mol^{-1}.

at the BCPs connecting the noble metal atoms. The extracted parameters, along with the interaction energies, are compiled in Tables 1 and 2.

Notably, for the argentophilic dimers, we observed energy values ranging from −5 to −9 kcal mol^{-1} in complexes **1–28**, and from −9 to −11 kcal mol^{-1} in complexes **29–42**. This variation suggests that the pyridine ligand either enhances the argentophilic interaction or contributes to the dimerization energy *via* long-range van der Waals forces. Another interesting observation is that the formation of dimers in those complexes with electron-withdrawing substituents are more favourable compared to those with electron-donating groups. Furthermore, the energy analysis of complexes **1–21** indicates that the interaction strength of argentophilic bonds increases with the atomic weight of the halogen atom involved.

To analyse the effect of relativistic effects, Table 1 also gathers the interaction energies without applying the exact two-component (X2C) method for relativistic corrections in DFT calculations, and using the def2-TZVP basis set. Unexpectedly, the comparison revealed minimal differences between energies with and without relativistic corrections (Table 1), thus

suggesting that the PBE0-D4/def2-TZVP level of theory can be also used for studying argentophilic interactions.

To explore the predictive capability of the QTAIM parameters for argentophilic interactions, we evaluated the relevance of density (ρ), potential energy density (V), and Lagrangian kinetic energy density (G), alongside the Laplacian of the electron density ($\nabla^2\rho$). Regression analyses for Ag···Ag dimers, excluding complexes with R = H (**1**, **8**, **15**, **22**, **29**, and **36**), which served for method validation, are depicted in Fig. 4. We selected this set to have a representation of each series and minimize the influence of substituents. Notably, ρ (red dots), V (blue dots) and G (pink dots) exhibit good correlations with binding energies, with regression coefficients of 0.970, 0.960 and 0.958 respectively, suggesting their ability in predicting interaction energies, consistent with previous studies on halogen and chalcogen bonds.[60]

Furthermore, the correlation using $\nabla^2\rho$ ($r = 0.953$, green dots) also demonstrates the predictive utility of QTAIM for argentophilic interactions, with ρ proving most effective due to its highest regression coefficient and minimal standard deviation (SD = 0.43 kcal mol^{-1}). Consequently, we propose eqn (1)

$$E(\text{kcal mol}^{-1}) = -850.66 \times \rho(\text{a.u.}) + 11.17, \qquad (1)$$

for estimating argentophilic interaction strength.

Validation against energies of complexes not initially used in the regression plots (**1**, **8**, **15**, **22**, **29**, and **36**), see Table 2, revealed close agreement, with a maximum deviation of 0.61 kcal mol^{-1} for compound **15** and an SD of 0.31 kcal mol^{-1}, underscoring the accuracy of eqn (1). Furthermore, adding these complexes to the training set had a minimal impact on the equation and the correlation coefficient ($r = 0.972$ and
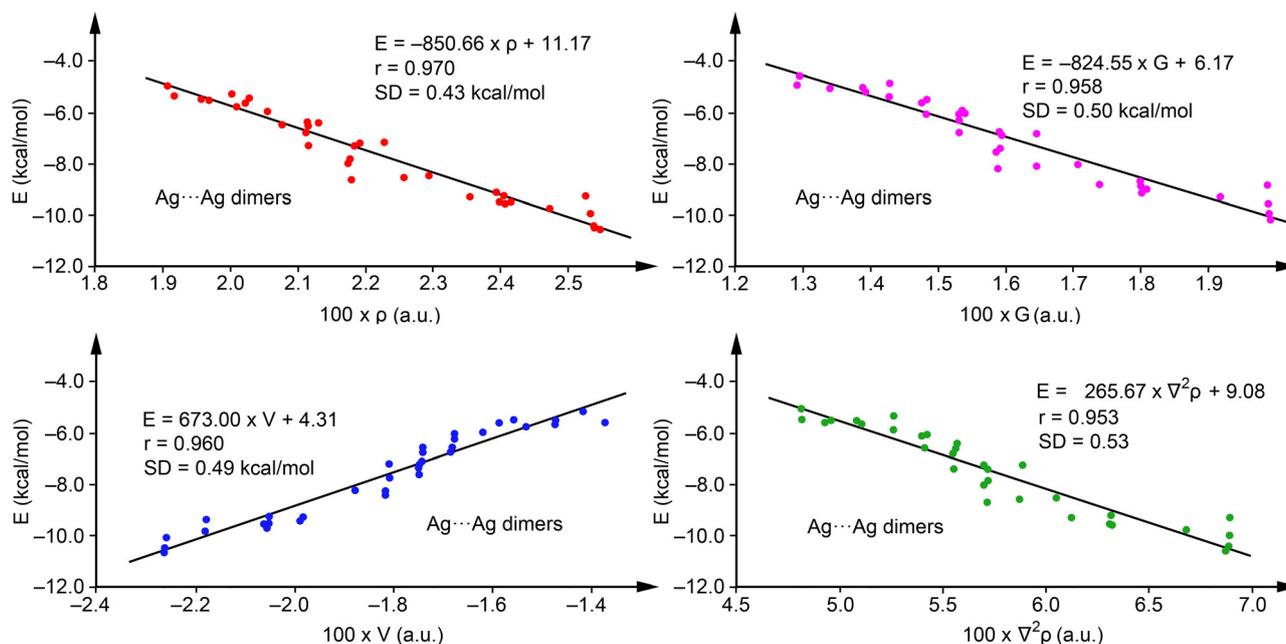
Fig. 4 Regression plots for Energy *versus* ρ (red) and $V(r)$ (blue), $G(r)$ (pink) and $\nabla^2\rho$ (green) for complexes **1–42**.

16554 | *Phys. Chem. Chem. Phys.*, 2024, **26**, 16550–16560

This journal is © the Owner Societies 2024

$E = -846.11 \times \rho + 11.04$), confirming the robustness of the regression model. Although our primary goal was simplicity, further analyses with multivariable models were performed showing the same or even worse correlation coefficient when using combination of two variables (V and G behave the best with $r = 0.970$, identical to eqn (1)), not justifying the use of more complicated equations. Curiously, worse correlation compared to eqn (1) was observed using three or more variables. More details are given in the ESI,† see Tables S1 and S2.

Gold complexes

A parallel study has been performed for gold complexes. Table 3 gathers the energetic features and topological parameters for complexes **43–84**. The main difference with the Ag complexes is that the energies are weaker, ranging from –4.3 to –9.2 kcal mol^{-1}. Previous results have shown that argentophilic interactions are stronger than aurophilic.[61] The data of Table 3 also discloses that Au···Au dimers with pyridine as ligand are stronger than those with nitrile and that electron withdrawing substituents favour the interaction, as also observed for Ag···Ag complexes. A notable distinction between Ag and Au complexes lies in the impact of incorporating relativistic effects on their binding energies. While the differences observed in Ag complexes were minimal, the effect is markedly significant for Au complexes ($\sim$1 kcal mol^{-1}). For instance, the inclusion of relativistic effects alters the binding energy of compound **57** by 1.4 kcal mol^{-1}, accounting for 19% of its total binding energy.

Fig. 5 showcases regression plots for Au···Au complexes **43–84**, plotting energy against the four QTAIM parameters for a comparative analysis with Ag complexes illustrated in Fig. 4. For method validation purposes, complexes with R = H (**43, 50, 57, 64, 71,** and **78**) were omitted from this analysis. It is observed that correlations for electron density (red dots), potential energy density (blue dots), Lagrangian kinetic energy density (pink dots), and the Laplacian of ρ (green dots) in the Au complexes are less robust than those observed in Ag complexes but still maintain acceptable levels of correlation. For the Au···Au complexes, the regression coefficients presented in Fig. 5 indicate that the interaction energy has a comparable correlation with all four QTAIM parameters examined, showcasing r values between 0.925 and 0.938, and standard deviation (SD) values spanning 0.51 to 0.56 kcal mol^{-1}. Given the slightly superior correlation coefficient for electron density, we propose the following equation for predicting the strength of aurophilic interactions:

$$E(\text{kcal mol}^{-1}) = -688.65 \times \rho(\text{a.u.}) + 10.03 \quad (2)$$

These findings indicate that employing QTAIM parameters to predict aurophilic interactions, as demonstrated in the regressions of Fig. 5, is plausible. However, such predictions should be approached with more caution than those of Ag. The validation against energies of complexes not initially used in the regression plots (**43, 50, 57, 64, 71,** and **78**) revealed a good agreement, with maximum deviation of 0.47 kcal mol^{-1} for compound **57** and a SD of 0.35 kcal mol^{-1}, underscoring the

Table 3 Dimerization energy (kcal mol^{-1}), distances (d, Å), ρ (a.u.), $\nabla^2\rho$ (a.u.), potential energy density (V, a.u.) and Lagrangian kinetic energy (G, a.u.) for complexes **43–84** at the PBE0(x2c)-D4/x2c-TZVPall level of theory

Dimer	E^a	d	ρ	$\nabla^2\rho$	V	G
43	−5.29 (−4.43)	3.188	0.0217	0.0543	−0.0141	0.0138
44	−5.73 (−4.83)	3.150	0.0231	0.0596	−0.0154	0.0152
45	−5.82 (−4.92)	3.175	0.0222	0.0561	−0.0145	0.0143
46	−5.77 (−4.81)	3.175	0.0222	0.0561	−0.0145	0.0143
47	−5.05 (−4.25)	3.175	0.0221	0.0560	−0.0145	0.0142
48	−4.32 (−3.57)	3.175	0.0220	0.0560	−0.0144	0.0142
49	−5.15 (−4.35)	3.163	0.0225	0.0577	−0.0149	0.0147
50	−5.96 (−4.92)	3.150	0.0232	0.0596	−0.0154	0.0152
51	−6.46 (−5.38)	3.125	0.0242	0.0633	−0.0164	0.0161
52	−6.55 (−5.48)	3.150	0.0232	0.0596	−0.0155	0.0152
53	−6.50 (−5.38)	3.163	0.0227	0.0577	−0.0150	0.0147
54	−5.74 (−4.78)	3.150	0.0231	0.0595	−0.0154	0.0152
55	−5.02 (−4.10)	3.150	0.0230	0.0595	−0.0154	0.0151
56	−5.87 (−4.89)	3.138	0.0236	0.0613	−0.0159	0.0156
57	−7.18 (−5.78)	3.125	0.0243	0.0633	−0.0165	0.0162
58	−7.74 (−6.29)	3.088	0.0260	0.0694	−0.0182	0.0178
59	−7.81 (−6.40)	3.113	0.0249	0.0654	−0.0171	0.0167
60	−7.73 (−6.27)	3.125	0.0244	0.0633	−0.0165	0.0162
61	−7.00 (−5.69)	3.125	0.0243	0.0632	−0.0165	0.0162
62	−6.28 (−5.01)	3.125	0.0242	0.0632	−0.0165	0.0161
63	−7.14 (−5.80)	3.113	0.0248	0.0652	−0.0170	0.0167
64	−5.58 (−4.47)	3.163	0.0229	0.0581	−0.0150	0.0148
65	−5.82 (−4.70)	3.150	0.0234	0.0598	−0.0155	0.0152
66	−5.92 (−4.80)	3.163	0.0230	0.0581	−0.0151	0.0148
67	−5.78 (−4.61)	3.150	0.0235	0.0599	−0.0155	0.0152
68	−5.60 (−4.55)	3.163	0.0228	0.0580	−0.0150	0.0148
69	−5.03 (−4.03)	3.175	0.0223	0.0562	−0.0145	0.0143
70	−5.64 (−4.58)	3.163	0.0228	0.0580	−0.0150	0.0148
71	−8.44 (−7.53)	3.063	0.0274	0.0743	−0.0196	0.0191
72	−8.41 (−7.51)	3.075	0.0268	0.0720	−0.0190	0.0185
73	−9.04 (−8.13)	3.063	0.0274	0.0743	−0.0196	0.0191
74	−8.90 (−7.97)	3.075	0.0268	0.0721	−0.0190	0.0185
75	−8.20 (−7.33)	3.063	0.0273	0.0743	−0.0196	0.0191
76	−7.39 (−6.57)	3.063	0.0273	0.0742	−0.0196	0.0191
77	−8.19 (−7.32)	3.063	0.0273	0.0743	−0.0196	0.0191
78	−8.97 (−7.82)	3.075	0.0270	0.0722	−0.0191	0.0186
79	−9.00 (−7.86)	3.075	0.0270	0.0723	−0.0191	0.0186
80	−9.18 (−8.05)	3.075	0.0271	0.0723	−0.0191	0.0186
81	−9.21 (−8.05)	3.075	0.0271	0.0723	−0.0191	0.0186
82	−8.99 (−7.86)	3.063	0.0276	0.0745	−0.0197	0.0192
83	−8.28 (−7.20)	3.075	0.0269	0.0722	−0.0190	0.0185
84	−8.77 (−7.66)	3.075	0.0270	0.0722	−0.0191	0.0186

^{a} Energies in parenthesis were computed using the PBE0-D4/def2-TZVP level of theory. The repression plots for this level of theory are included in the ESI, Fig. S2.

applicability of eqn (2) (see Table 4). Similarly to the Ag-complexes, adding these complexes to the training set had a minimal impact on the equation and the correlation coefficient ($r = 0.943$, $E = -681.57 \times \rho + 9.84$).

Multivariable analysis indicates that incorporating two variables does not enhance the regression coefficient, while including three variables (ρ, V, and G) slightly improves it to $r = 0.960$. This leads to the formulation of eqn (3)

$$E(\text{kcal mol}^{-1}) = -2533.14 \times \rho(\text{a.u.}) + 12\,737.86 \times V(\text{a.u.})$$
$$+ 15\,562.41 \times G(\text{a.u.}) + 13.56 \quad (3)$$

with a standard deviation (SD) of 0.39 kcal mol^{-1}. This equation also yields a lower standard deviation than eqn (2) when estimating the energies of complexes **43, 50, 57, 64, 71,** and **78**,

This journal is © the Owner Societies 2024

Phys. Chem. Chem. Phys., 2024, **26**, 16550–16560 | **16555**
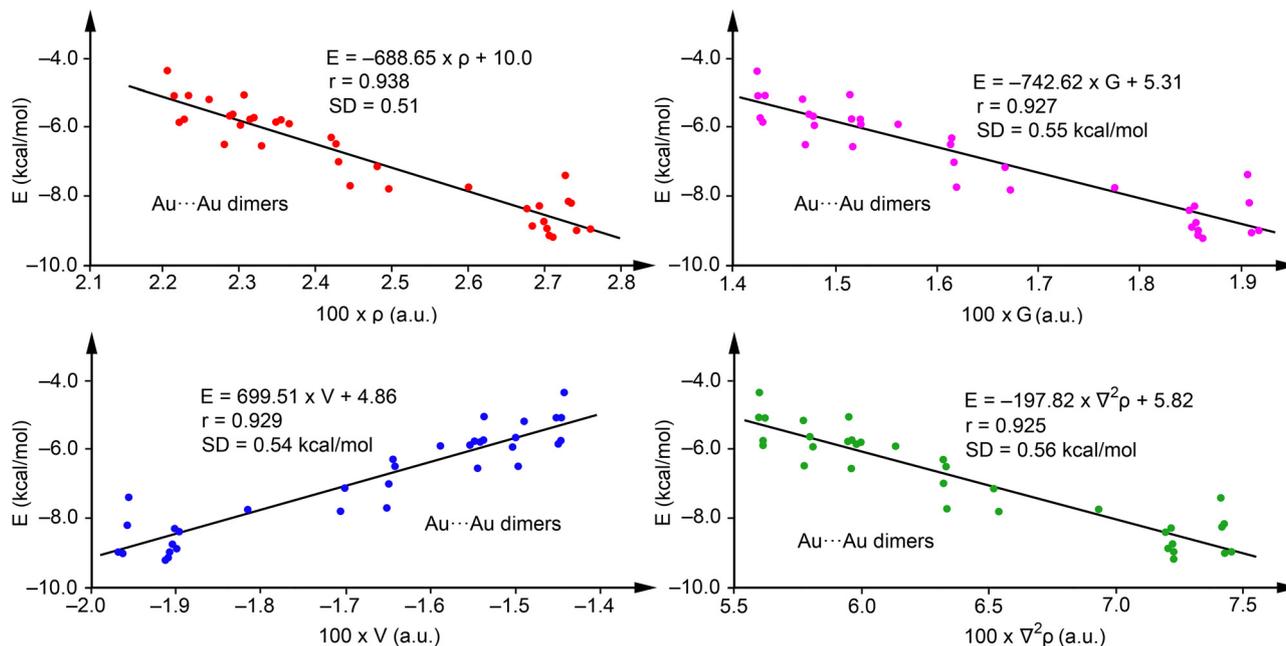
Fig. 5 Regression plots for Energy *versus* ρ (red) and $V(r)$ (blue), $G(r)$ (pink) and $\nabla^2\rho$ (green) for complexes **43–84**.

Table 4 Dimerization energies (kcal mol^{-1}) of complexes **1**, **8**, **15**, **22**, **29** and **36** using the scan plots (E), eqn (2) and eqn (3). The differences (ΔE, absolute value) are also indicated

Dimer	E	E (eqn (2))^a	E (eqn (3))^b	$|\Delta E|$ (eqn (2))	$|\Delta E|$ (eqn (3))
43	−5.29	−4.88	−5.33	0.41	0.04
50	−5.96	−5.92	−5.80	0.04	0.16
57	−7.18	−6.71	−6.84	0.47	0.34
64	−5.58	−5.74	−6.05	0.16	0.47
71	−8.44	−8.81	−8.53	0.37	0.09
78	−8.97	−8.57	−9.01	0.39	0.04

^{a} SD = 0.35 kcal mol^{-1}. ^{b} SD = 0.27 kcal mol^{-1}.

with the largest discrepancy being 0.47 kcal mol^{-1} for complex **64** and an SD of 0.27 kcal mol^{-1}. Given that both equations show acceptable discrepancies below 0.5 kcal mol^{-1} and that eqn (2) offers a simpler alternative, we recommend using eqn (2) as the more convenient predictor for aurophilic interactions. The marginal improvement offered by eqn (3) does not warrant the complexity of using a more cumbersome formula.

Physical interpretation of the equations

The electron density represents the distribution of electrons in the space around an atom or molecule, derived from the wavefunction that defines the chemical entity. Consequently, the electron density around a molecule is influenced by the atomic nuclei that constitute the molecule. As two molecules, initially far apart, come closer together, their electronic clouds merge and modify the electronic space around them. Consequently, any bonding interaction between two atoms is exhibited in the electron density distribution [$\rho(r)$] as a topological saddle conformation around the interatomic zero-flux surface (S). At S, bond critical points (BCPs) appear, where the gradient

of density vanishes ($\nabla\rho(r) = 0$), and the electron density is a minimum in the direction parallel to the bond and a maximum in the perpendicular plane. Two gradient lines starting at the corresponding nuclei and ending at the BCP form the bond path, which is considered an identifier of the interaction.[59]

We propose that the regression equations in our manuscript, which relate the interaction energies of Ag–Ag and Au–Au bonds to QTAIM parameters, serve as predictors for the strength of metallophilic interactions. The electron density at the BCP is a direct measure of the shared electronic charge between the two metal atoms. Higher ρ values indicate stronger interactions due to greater electron sharing or delocalization, reflecting a more substantial attractive force between the atoms. Additionally, other properties at the BCP, derived from the electron density, such as the Laplacian of the electron density ($\nabla^2\rho$), the Lagrangian kinetic energy density (G), the potential energy density (V), and the total energy density (H), should also be directly related to the strength of the interaction between the two metal centres. In fact, the kinetic and potential energy densities at the BCP are related to the Laplacian by the local form of the virial theorem: $\frac{1}{4}\nabla^2\rho = 2G + V$. Moreover, it has been previously demonstrated that G and V are mostly influenced by the Pauli repulsion and the stabilizing effect of the electric field, respectively.[52–54]

As representative case, Fig. 6 illustrates complex **4** at different distances between the Ag$\cdots$Ag centres. Starting from 5.0 Å and decreasing to the energetic minimum at 3.0125 Å, the electron density is represented, and the progressive merging of the electron clouds of both units gives rise to a bond path and a BCP between the Ag$\cdots$Ag centres. The values of ρ, $\nabla^2\rho$, $|V|$, and G progressively increase as the distance reaches the energy minimum (see Table S3, ESI†). This demonstrates that the
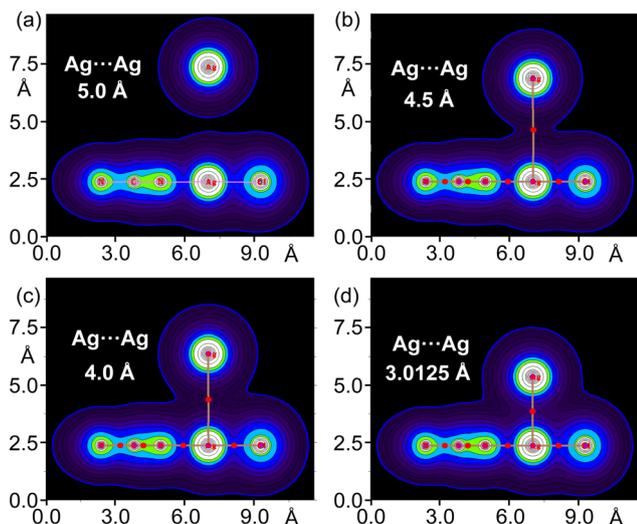
16556 | *Phys. Chem. Chem. Phys.*, 2024, **26**, 16550–16560

This journal is © the Owner Societies 2024

Fig. 6 2D plots of the electron density of the dimer **4** at 5.0 Å, (a); 4.5 Å (b); 4.0 Å, (c) and at the energetic minimum 3.0125 Å, (d). For (b)−(d), the resulting BCPs and bond paths interconnecting the Ag-atoms are depicted in red and light brown colours, respectively.

electron density at the BCP between the regium metals is proportional to the interaction energies of the two monomers, and consequently, the strength of the metallophilic force.

Application of eqn (1) and (2)

The equations developed in this study were applied to all examples featured in Fig. 1 and 2. For the Ag compounds, we calculated the dimerization energies for **BIQWEF**, **HAMMIS**, **POKHEE**, and **YUXVUJ**, accompanied by QTAIM analyses as illustrated in Fig. 7. Additionally, for **HAMMIS** (which also serves as a model for the related **LURDIM** structure), we calculated the interaction energies, including the counterions. For clarity, the counterions are not depicted in Fig. 7b; however, the complete assembly can be viewed in the ESI,† Fig. S3. In **BIQWEF**, QTAIM analysis identified three bond critical points (BCPs, small red spheres) and bond paths (solid orange lines) linking the monomers, with two BCPs corresponding to NH···Cl hydrogen bonds and one to an argentophilic interaction (Fig. 7a). The substantial dimerization energy (-29.5 kcal mol^{-1}) results from these combined interactions, likely augmented by electrostatic attraction between Cl and Ag atoms. The contribution from the Ag···Ag interaction in the dimer is quantified as -1.0 kcal mol^{-1}. QTAIM analysis for **HAMMIS** reveals only one BCP connecting the two Ag atoms, indicating that the argentophilic interaction is the sole link between the monomers. The binding energy is repulsive at 69.4 kcal mol^{-1} due to the electrostatic repulsion between the cationic monomers. However, when counterions are included in the calculations, the assembly formation, as shown in Fig. S3 (ESI†), it becomes energetically favorable at -117.9 kcal mol^{-1}. Using the equation developed in this study, the argentophilic contribution is calculated as -3.5 kcal mol^{-1}. For **POKHEE** (Fig. 7c), QTAIM analysis identifies four BCPs and bond paths linking the neutral monomers, with three BCPs corresponding
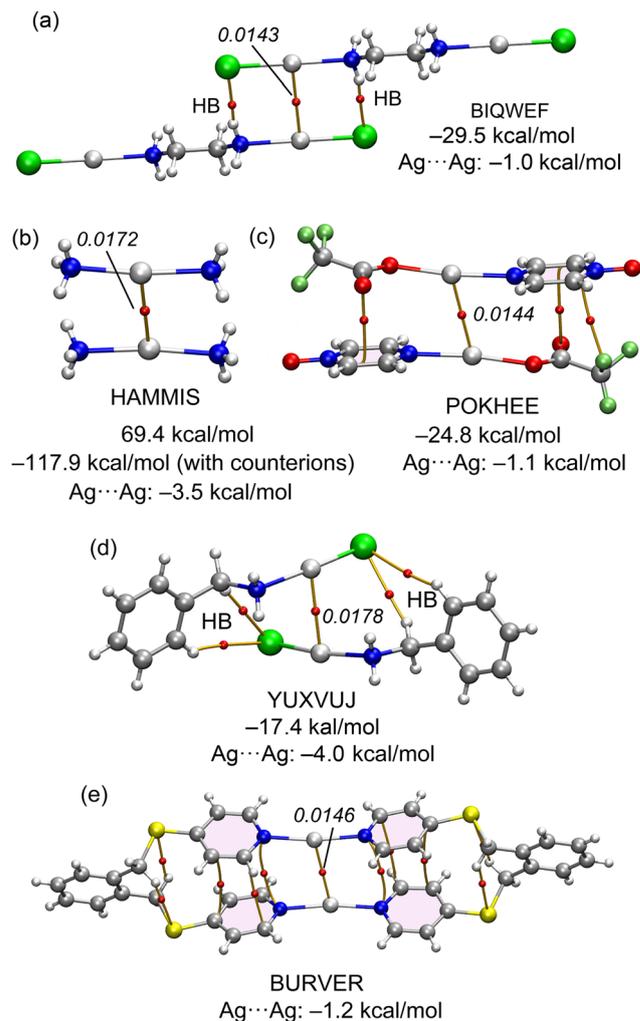

Fig. 7 QTAIM analyses of **BIQWEF** (a), **HAMMIS** (b), **POKHEE** (c), **YUXVUJ** (d) and **BURVER** (e). The density values are given in italics. Dimerization energies and argentophilic energies are also indicated.

to anion–π interactions[60] and one to an argentophilic interaction. The dimerization energy is -24.8 kcal mol^{-1}, with the Ag···Ag interaction contributing -1.1 kcal mol^{-1}, highlighting the dominance of anion–π interactions in this system.[62] In **YUXVUJ**, QTAIM analysis reveals several CH···Cl contacts in addition to the argentophilic interaction, resulting in a total of five BCPs and bond paths that connect the monomers.

The calculated dimerization energy for **YUXVUJ** is -17.6 kcal mol^{-1}, with the Ag···Ag interactions contributing -4.0 kcal mol^{-1}. For the **BURVER** dinuclear complex (Fig. 6e), the intramolecular argentophilic interaction is estimated at -1.2 kcal mol^{-1}. Additionally, QTAIM analysis in **BURVER** reveals two π-stacking interactions, represented by six bond critical points (BCPs) interconnecting the aromatic rings, and four CH···S contacts. Each CH···S contact is characterized by a BCP and bond path linking the hydrogen and sulfur atoms.

For the Au complexes, we began our analysis with the **GOGFIR** structure, in which the monomers are neutral. This structure demonstrates a dimerization energy of -29.0 kcal mol^{-1},
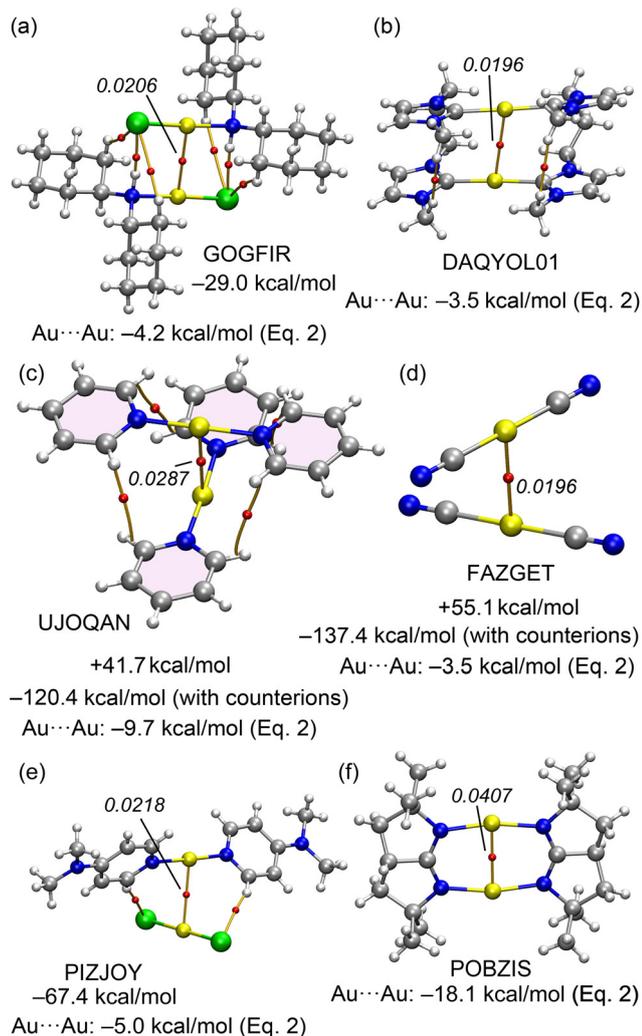
This journal is © the Owner Societies 2024

Phys. Chem. Chem. Phys., 2024, **26**, 16550–16560 | **16557**

(a)

0.0206

GOGFIR
−29.0 kcal/mol

Au···Au: −4.2 kcal/mol (Eq. 2)

(b)

0.0196

DAQYOL01

Au···Au: −3.5 kcal/mol (Eq. 2)

(c)

0.0287

UJOQAN

+41.7 kcal/mol

−120.4 kcal/mol (with counterions)

Au···Au: −9.7 kcal/mol (Eq. 2)

(d)

0.0196

FAZGET
+55.1 kcal/mol
−137.4 kcal/mol (with counterions)

Au···Au: −3.5 kcal/mol (Eq. 2)

(e)

0.0218

PIZJOY
−67.4 kcal/mol

Au···Au: −5.0 kcal/mol (Eq. 2)

(f)

0.0407

POBZIS

Au···Au: −18.1 kcal/mol (Eq. 2)

Fig. 8 QTAIM analyses of **GOGFIR** (a), **DAQYOL01** (b), **UJOQAN** (c), **FAZGET** (d), **PIZJOY** (e) and **POBZIS** (f). The density values are given in italics. Dimerization energies with and without the counterions and aurophilic energies are also indicated.

attributable primarily to the aurophilic interaction, supplemented by four additional contacts (two CH···Cl and two NH···Cl). QTAIM analysis has identified corresponding BCPs and bond paths for these interactions. The substantial dimerization energy of −29.0 kcal mol^{-1} includes an aurophilic contribution of −4.2 kcal mol^{-1}, as calculated from eqn (2). In the case of **DAQYOL01** (Fig. 8b), the Au···Au contact is intramolecular and thus not amenable to estimation using the supramolecular approach typically employed. Instead, the strength of this Au···Au contact, estimated using eqn (2), is −3.5 kcal mol^{-1}. The cation···cation and anion···anion dimer pairs from the CSD with reference codes **UJOQAN** and **FAZGET** were also analysed (see Fig. 8c and d). QTAIM analysis for **UJOQAN** revealed a BCP connecting the Au atoms, confirming the aurophilic interaction.

Additionally, four BCPs and bond paths interconnecting the aromatic H-atoms of pyridine rings suggest the presence of

ancillary van der Waals interactions. In contrast, the **FAZGET** structure exhibits solely the aurophilic interaction, as denoted by its BCP and bond path (Fig. 8). In both instances, the dimerization energies are repulsive, reflecting the coulombic repulsion between ions of identical charge. However, upon including counterions in the calculations (tetrafluoroborate for **UJOQAN** and triazolium for **FAZGET**, see Fig. S3 in ESI† for the computed assemblies), the formation energies turn significantly negative, attributed to the strong attractions between anions and cations. Thus, any of both interactions energies is not useful to underscore the significance of the aurophilic contact strength. Using eqn (2), the contributions from aurophilic interactions are estimated at −9.7 kcal mol^{-1} for **UJOQAN** and −3.5 kcal mol^{-1} for **FAZGET**, consistent with the findings of Table 3 that evidence that pyridine ligands exhibit stronger interactions than cyanide. The ion pair interaction in **PIZJOY** has also been investigated. The QTAIM analysis reveals that the anion and cation are linked by three bond critical points (BCPs) and bond paths, involving two CH···Cl and one Au···Au contacts. The interaction energy is notably substantial, primarily due to the pure Coulombic attraction, measuring at −67.4 kcal mol^{-1}. The aurophilic interaction, as calculated from eqn (2), is −5.0 kcal mol^{-1}. In the case of **POBZIS**, the intramolecular Au···Au interaction is significantly stronger, estimated at −18.1 kcal mol^{-1}. This is largely attributed to the high value of electron density (ρ = 0.0407 a.u.) at the BCP. However, this estimation of the aurophilic interaction should be approached with caution, as this ρ value significantly exceeds the range used to develop eqn (2), potentially affecting the accuracy of this estimation.

Conclusions

Based on the findings of our study, we can draw several key conclusions:

1. The interaction energies of argentophilic bonds can be predicted using the charge density (ρ) at the bond critical points (BCPs), as evidenced by strong correlations in our data. We recommend using the equation E_{int}(kcal mol^{-1}) = −850.66 × ρ(a.u.) + 11.17 for such predictions.

2. Similarly, we observed reliable correlations for aurophilic interactions, indicating that QTAIM parameters are also effective for estimating these interactions. We suggest the equation E_{int}(kcal mol^{-1}) = −688.65 × ρ(a.u.) + 10.03.

3. Our proposed methodology provides a simple and effective way to calculate Rg···Rg interaction energies (Rg = Ag or Au) for both intramolecular and charged system interactions. This method circumvents the complexities of more elaborate modelling techniques.

4. The application of a relativistic Hamiltonian along with all-electron relativistic basis sets shows minimal impact on Ag···Ag dimer calculations but significantly affects the results for Au···Au complexes, underscoring the importance of considering relativistic effects, particularly for gold-based interactions.

Author contributions

The manuscript was collaboratively developed with contributions from all authors.

Conflicts of interest

There are no conflicts to declare.

Acknowledgements

Notes and references

1 F. Huang and V. Anslyn, *Chem. Rev.*, 2015, **115**, 6999–7000.
2 H. Schmidbaur and A. Schier, *Chem. Soc. Rev.*, 2012, **41**, 370–412.
3 H. Schmidbaur and A. Schier, *Angew. Chem. Int. Ed.*, 2015, **54**, 746–784.
4 S. Sculfort and P. Braunstein, *Chem. Soc. Rev.*, 2011, **40**, 2741.
5 V. W.-W. Yam and E. C.-C. Cheng, *Top. Curr. Chem.*, 2007, **281**, 269.
6 M. Bardaji and A. Laguna, *J. Chem. Educ.*, 1999, **76**, 201.
7 H. Schmidbaur and A. Schier, *Chem. Soc. Rev.*, 2008, **37**, 1931.
8 S. S. Pathaneni and G. R. Desiraju, *J. Chem. Soc., Dalton Trans.*, 1993, 319.
9 L. Magnko, M. Schweizer, G. Rauhut, M. Schütz, H. Stoll and H.-J. Werner, *Phys. Chem. Chem. Phys.*, 2002, **4**, 1006.
10 K. M. Anderson, A. E. Goeta and J. W. Steed, *Inorg. Chem.*, 2007, **46**, 6444.
11 P. Pyykkö, *Chem. Rev.*, 1988, **88**, 563.
12 P. Pyykkö, *Chem. Rev.*, 1997, **97**, 597.
13 P. Pyykkö, *Angew. Chem., Int. Ed.*, 2004, **43**, 4412.
14 P. Pyykkö, *Inorg. Chim. Acta*, 2005, **358**, 4113.
15 P. Pyykkö, *Chem. Soc. Rev.*, 2008, **37**, 1967.
16 N. Mirzadeh, S. H. Privér, A. J. Blake, H. Schmidbaur and S. K. Bhargava, *Chem. Rev.*, 2020, **120**, 7551–7591.
17 M. Pujadas and L. Rodríguez, *Coord. Chem. Rev.*, 2020, **408**, 213179.
18 A. Pinto, N. Svahn, J. C. Lima and L. Rodríguez, *Dalton Trans.*, 2017, **46**, 11125–11139.
19 V. W. W. Yam, V. K. M. Au and S. Y. L. Leung, *Chem. Rev.*, 2015, **115**, 7589–7728.
20 J. C. Lima and L. Rodríguez, *Chem. Soc. Rev.*, 2011, **40**, 5442–5456.
21 D. Weber and M. R. Gagné, *Top. Curr. Chem.*, 2015, **357**, 167–211.
22 E. Priola, A. Giordana, R. M. Gomila, E. Zangrando, L. Andreo, R. Rabezzana, L. Operti, E. Diana, G. Mahmoudi and A. Frontera, *Dalton Trans.*, 2022, **51**, 5818–5827.
23 J. Romanova, M. R. Ranga Prabhath, Y. Sadik and P. D. Jarowski, in Quantum Systems in Physics, Chemistry, and Biology, *Progress in Theoretical Chemistry and Physics*, ed. A. Tadjer, R. Pavlov, J. Maruani, E. Brändas and G. Delgado-Barrio, Springer, Cham, 2017, Vol. 30.
24 Q. Zhang, Q. Wang, X.-X. Chen, P. Zhang, C.-F. Ding, Z. Li and Y.-B. Jiang, *TrAC, Trends Anal. Chem.*, 2018, **109**, 32–42.
25 S. Komori, K. Tada, N. Taguchi, T. Taniyama and T. Masese, *J. Mater. Chem. C*, 2023, **11**, 11213–11217.
26 X.-Q. Zhou, P. Wang, V. Ramu, L. Zhang, S. Jiang, X. Li, S. Abyar, P. Papadopoulou, Y. Shao, L. Bretin, M. A. Siegler, F. Buda, A. Kros, J. Fan, X. Peng, W. Sun and S. Bonnet, *Nat. Chem.*, 2023, **15**, 980–987.
27 M. J. Katz, K. Sakai and D. B. Leznoff, *Chem. Soc. Rev.*, 2008, **37**, 1884–1895.
28 (*a*) E. Priola, G. Mahmoudi, J. Andreo and A. Frontera, *Chem. Commun.*, 2021, **57**, 7268; (*b*) J. Echeverría, *CrystEngComm*, 2018, **20**, 3987.
29 P. Niermeier, L. Wickemeyer, B. Neumann, H.-G. Stammler, L. Goett-Zink, T. Kottke and N. W. Mitzel, *Dalton Trans.*, 2019, **48**, 4109.
30 J. M. Guevara-Vela, K. Hess, T. Rocha-Rinza, Á. Martín Pendás, M. Flores-Álamo and G. Moreno-Alcántar, *Chem. Commun.*, 2022, **58**, 1398.
31 T. Seki, K. Ida and H. Ito, *Mater. Chem. Front.*, 2018, **2**, 1195.
32 (*a*) C. Adamo and V. Barone, *J. Chem. Phys.*, 1999, **110**, 6158–6170; (*b*) D. Peng, N. Middendorf, F. Weigend and M. Reiher, *J. Chem. Phys.*, 2013, **138**, 184105.
33 (*a*) E. Caldeweyher, C. Bannwarth and S. Grimme, *J. Chem. Phys.*, 2017, **147**, 034112; (*b*) E. Caldeweyher, J.-M. Mewes, S. Ehlert and S. Grimme, *Phys. Chem. Chem. Phys.*, 2020, **22**, 8499–8512.
34 (*a*) Y. J. Franzke, R. Treß, T. M. Pazdera and F. Weigend, *Phys. Chem. Chem. Phys.*, 2019, **21**, 16658–16664; (*b*) F. Weigend, *Phys. Chem. Chem. Phys.*, 2006, **8**, 1057–1065.
35 M. Dolg, H. Stoll, A. Savin and H. Preuss, *Theor. Chim. Acta*, 1989, **75**, 173–194.
36 M. Kaupp, P. V. Schleyer, H. Stoll and H. Preuss, *J. Chem. Phys.*, 1991, **94**, 1360–1366.
37 R. Ahlrichs, M. Bär, M. Häser, H. Horn and C. Kömel, *Chem. Phys. Lett.*, 1989, **162**, 164–169.
38 R. F. W. Bader, *Chem. Rev.*, 1991, **91**, 893–928.
39 T. Lu and F. Chen, *J. Comput. Chem.*, 2012, **33**, 580–592.
40 K. Binnemans, N. R. Brooks, D. Depuydt, L. Van Meervelt, S. Schaltin and J. Fransaer, *ChemPlusChem*, 2013, **78**, 578.
41 Z.-L. You, H.-L. Zhu and W.-S. Liu, *Acta Crystallogr., Sect. E: Struct. Rep. Online*, 2004, **60**, m1903.
42 D. Sun, N. Zhang, G.-G. Luo, Q.-J. Xu, R.-B. Huang and L.-S. Zheng, *Polyhedron*, 2010, **29**, 1842.
43 R. Puttreddy, J. R. A. Cottam and P. J. Steel, *RSC Adv.*, 2014, **4**, 22449.
44 C. Wolper, M. D. P. Bastardes, I. Dix, D. Kratzert and P. G. Jones, *Z. Naturforsch., B: J. Chem. Sci.*, 2010, **65**, 647.

This journal is © the Owner Societies 2024

Phys. Chem. Chem. Phys., 2024, **26**, 16550–16560 | **16559**

45 H. Xue, F. Jiang, Q. Chen, D. Yuan, J. Pang, G. Lv, X. Wan, L. Liang and M. Hong, *Chem. Commun.*, 2015, **51**, 13706.

46 P. G. Jones and B. Ahrens, *New J. Chem.*, 1998, **22**, 1041.

47 J. C. Y. Lin, S. S. Tang, C. S. Vasam, W. C. You, T. W. Ho, C. H. Huang, B. J. Sun, C. Y. Huang, C. S. Lee, W. S. Hwang, A. H. H. Chang and I. J. B. Lin, *Inorg. Chem.*, 2008, **47**, 2543.

48 R. Corbo, G. F. Ryan, M. A. Haghighatbin, C. F. Hogan, D. J. D. Wilson, M. D. Hulett, P. J. Barnard and J. L. Dutton, *Inorg. Chem.*, 2016, **55**, 2830.

49 W. Dong, Y.-Q. Sun, B. Yu, H.-B. Zhou, H.-B. Song, Z.-Q. Liu, Q.-M. Wang, D.-Z. Liao, Z.-H. Jiang, S.-P. Yan and P. Cheng, *New J. Chem.*, 2004, **28**, 1347.

50 M. Baron, C. Tubaro, A. Biffis, M. Basato, C. Graiff, A. Poater, L. Cavallo, N. Armaroli and G. Accorsi, *Inorg. Chem.*, 2012, **51**, 1778.

51 L. Tong, L. M. Davis, X. Gong, J. Feng, E. S. Beh and R. G. Gordon, *Dalton Trans.*, 2019, **48**, 6709.

52 E. Espinosa, E. Molins and C. Lecomte, *Chem. Phys. Lett.*, 1998, **285**, 170–173.

53 I. Mata, I. Alkorta, E. Espinosa and E. Molins, *Chem. Phys. Lett.*, 2011, **507**, 185–189.

54 I. Mata, E. Molins, I. Alkorta and E. Espinosa, *J. Chem. Phys.*, 2009, **130**, 044104.

55 M. A. Spackman, *Cryst. Growth Des.*, 2015, **15**, 5624–5628.

56 M. L. Kuznetsov, *Int. J. Quantum Chem.*, 2019, **119**, e25869.

57 M. A. Spackman, *Cryst. Growth Des.*, 2015, **15**, 5624–5628.

58 M. L. Kuznetsov, *Int. J. Quantum Chem.*, 2019, **119**, e25869.

59 A. Bauza and A. Frontera, *ChemPhysChem*, 2020, **21**, 26–31.

60 R. F. W. Bader, *J. Phys. Chem. A*, 1998, **102**, 7314–7323.

61 L. Ray, M. M. Shaikh and P. Ghosh, *Inorg. Chem.*, 2008, **47**, 230–240.

62 A. Frontera, P. Gamez, M. Mascal, T. J. Mooibroek and J. Reedijk, *Angew. Chem., Int. Ed.*, 2011, **50**, 9564–9583.

16560 | *Phys. Chem. Chem. Phys.*, 2024, **26**, 16550–16560

This journal is © the Owner Societies 2024